Photon production from gluon-mediated quark–anti-quark annihilation at confinement

Sarah Campbell*
Columbia University, Nevis Labs, Irvington, New York 10533, USA
(Received 8 April 2015; published 23 July 2015)

Heavy ion collisions at the BNL Relativistic Heavy Ion Collider produce direct photons at low transverse momentum p_T from 1–3 GeV/c, in excess of the $p+p$ spectra scaled by the nuclear overlap factor T_{AA}. These low-p_T photons have a large azimuthal anisotropy v_2. Theoretical models, including hydrodynamic models, struggle to quantitatively reproduce the large low-p_T direct photon excess and v_2 in a self-consistent manner. This paper presents a description of the low-p_T photon flow as the result of increased photon production from soft-gluon-mediated q-$\bar{q}$ interactions as the system becomes color neutral. This production mechanism will generate photons that follow constituent quark number, n_q, scaling of v_2 with an n_q value of 2 for direct photons. χ^2 comparisons of the published PHENIX direct photon and identified particle v_2 measurements finds that n_q scaling applied to the direct photon v_2 data prefers the value $n_q = 1.8$ and agrees with $n_q = 2$ within errors in most cases. The 0–20% and 20–40% Au+Au direct photon data are compared to a coalescence-like Monte Carlo simulation that calculates the direct photon v_2 while describing the shape of the direct photon p_T spectra in a consistent manner. The simulation, while systematically low compared to the data, is in agreement with the Au+Au measurement at p_T less than 3 GeV/c in both centrality bins. Furthermore, this production mechanism predicts that higher order flow harmonics v_n in direct photons will follow the modified n_q-scaling laws seen in identified hadron v_n with an n_q value of 2.

DOI: 10.1103/PhysRevC.92.014907 PACS number(s): 25.75.Dw

I. INTRODUCTION

Direct photons are all of the photons produced in a collision excluding the products of hadronic decays. They are emitted throughout the evolution of the heavy ion medium, and because they are color neutral they do not experience subsequent interactions with the medium. As a result, their spectrum provides a time-integrated picture of photon emission. Direct photons have various sources, including prompt photons generated by early hard parton interactions, photons produced in the pre-equilibrium stage, and thermal photons radiated from either the quark-gluon plasma (QGP) or the hadron gas stage (HG). In Fig. 1, Feynman diagrams of prompt photon production mechanisms, quark-gluon Compton scattering, quark–anti-quark annihilation, and bremsstrahlung radiation are shown. Prompt photons are created in $p+p$ collisions and dominate the yield at high p_T in heavy ion collisions. Prompt photon production rates can be calculated using perturbative QCD (pQCD); quark-gluon Compton scattering and quark–anti-quark annihilation have production rates of order $\alpha_S\alpha$ and bremsstrahlung radiation has a rate of order $\alpha_S^2\alpha$. QCD thermal photons have the same production diagrams, shown in Fig. 1, but with the partons thermalized in the medium. In thermal photon pQCD calculations, bremsstrahlung radiation is of order $\alpha_S\alpha$ and can exceed the production from the Compton scattering and annihilation processes. HG thermal photons have analogous production mechanisms to the Compton scattering and annihilation processes only with pions and ρ mesons interacting instead of quarks and gluons. However, the production rates for thermal photons and other direct photon sources are not well constrained particularly in the nonperturbative regime. This makes separating the contributions of direct photons at low and intermediate p_T difficult.

The PHENIX experiment discovered a large direct photon excess at low-p_T, from 1–3 GeV/c, in $\sqrt{s_{NN}} = 200$ GeV Au+Au collisions at the BNL Relativistic Heavy Ion Collider (RHIC) relative to the yields of direct photons in $p+p$ collisions scaled by the nuclear overlap factor T_{AA} [2,3]. Subsequent analyses found that these low-p_T photons, again from 1–3 GeV/c, have a large azimuthal anisotropy with respect to the collision's event plane [4]. Preliminary results from the ALICE experiment at the CERN Large Hadron Collider (LHC) suggest similar behavior in 2.76 TeV Pb+Pb collisions [5,6]. Hydrodynamic models are able to describe the direct photon yield with initial temperatures of 300–600 MeV and thermalization times between 0.15 and 0.5 fm/c [2]. Reproducing the large measured azimuthal anisotropies v_2 at these early times has proven difficult for hydrodynamic models [7–9]. This is because the large azimuthal anisotropies generated by hydrodynamic pressure gradients need time to develop. To address this puzzle some theories introduce delayed QGP formation [10], new sources of photon production involving strong magnetic fields [11,12], and initial state Glasma effects [13], while others consider increased contributions from the hadron gas stage due to baryon-baryon and meson-baryon interactions [14,15].

In this paper, the sources of identified hadron azimuthal anisotropies are considered to understand the origin of the similarly sized direct photon v_2. At low-p_T, bulk expansion dominates the hadronic v_2 while at high p_T, hadrons from jet fragmentation dominate. In the intermediate-p_T region, from 1–3 GeV/c, the measured baryon and meson v_2 values split, with baryons reaching higher values of v_2 at higher values of p_T [16]. When the baryon and meson v_2 values are scaled by their number of constituent quarks, n_q, a

*sc3877@columbia.edu

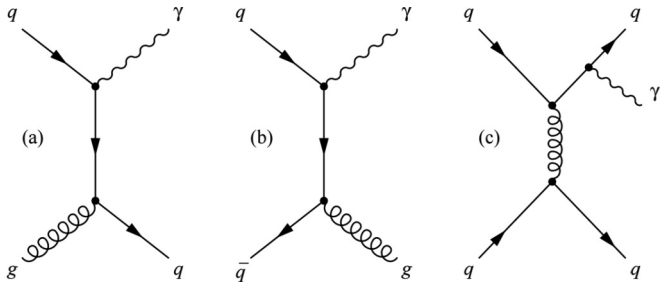

FIG. 1. Feynman diagrams of prompt photon production by (a) quark-gluon Compton scattering, (b) quark–anti-quark annihilation, and (c) bremsstrahlung radiation off of an outgoing quark [1].

uniform behavior between baryons and mesons is seen [17]. Coalescence models are able to reproduce quark number scaling by assuming that hadron production is dominated by the recombination of flowing partons. They assume that thermalized co-moving quarks of a given p_T will coalesce into mesons and baryons with n_q-times the p_T and n_q-times the v_2 where $n_q = 2$ for mesons and $n_q = 3$ for baryons. In this framework, energy-momentum conservation is maintained by the mean-field interaction resulting in soft gluon interactions with the medium [18].

Similar mean-field or soft gluon interactions could mediate quark–anti-quark annihilation as the system moves toward color neutrality, resulting in a large increase in photon production. These interactions (a diagram is shown in Fig. 2) would produce photons from partonic processes late in the system's evolution when quarks are flowing. One consequence of this production is that these photons should reproduce constituent quark number scaling with the value $n_q = 2$ for direct photons. Furthermore, this model provides a testable prediction that higher order flow harmonics, v_n, in direct photons should follow the n_q-scaling laws seen in identified hadron v_n [19] again with $n_q = 2$ for direct photons.

Section II determines the n_q for direct photons that best reproduces the quark number scaling seen in the identified hadron v_2 by using a χ^2 analysis of existing published data [4,20]. Section III details a coalescence-like Monte Carlo calculation that combined with the T_{AA}-scaled $p + p$ component is compared to the measured direct photon p_T spectrum and v_2 distribution. A two-component model is assumed where the low-p_T direct photon excess is primarily the result of quark–anti-quark annihilation mediated by mean-field or soft gluon interactions as the system becomes color neutral.

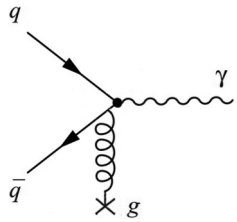

FIG. 2. Feynman diagram of the quark–anti-quark annihilation interaction with a medium gluon producing a direct photon.

II. n_q SCALING OF IDENTIFIED HADRON AND DIRECT PHOTON v_2

The elliptic flow of identified hadrons displays constituent quark number scaling in the 1–3 GeV/c p_T region [21,22]. In the q-$\bar{q}$ annihilation picture of direct photon production, this n_q-scaling behavior should extend to the direct photons with $n_q = 2$. This is because the n_q-scaled v_2 reflects the underlying anisotropy of the quarks and therefore is common for all hadrons and photons produced from these coalescing quarks. At high p_T, this n_q scaling may break down as contributions from hard processes begin to dominate in both the direct photon and identified hadron spectra. Figure 3 shows a comparison of the direct photon v_2 [4] with the charged pion, kaon, and proton v_2 [20] in the 0–20% and 20–40% $\sqrt{s_{NN}} = 200$ GeV Au+Au collisions. The n_q-scaled v_2 as a function of the n_q-scaled p_T

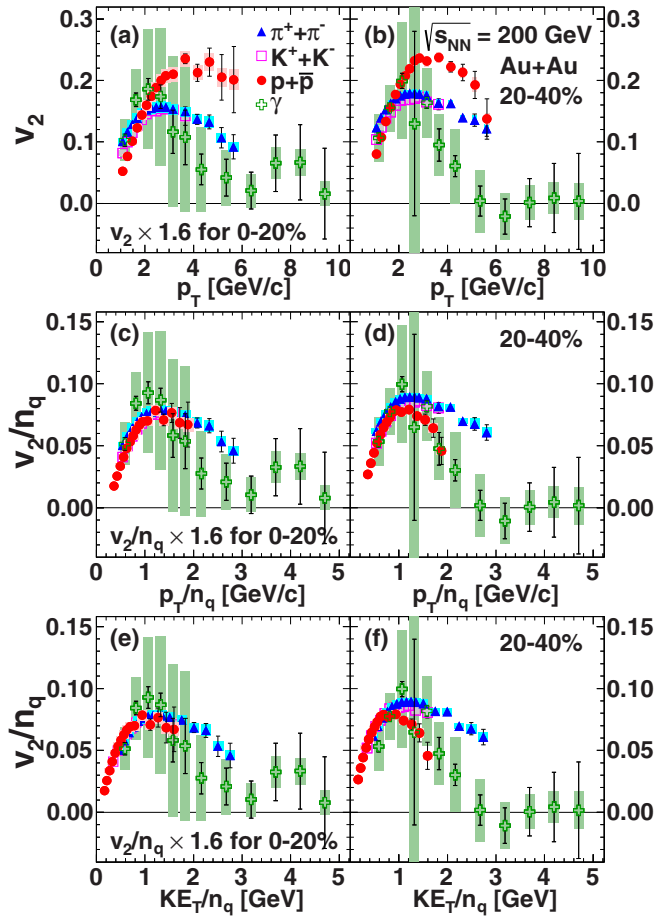

FIG. 3. (Color online) The π (blue triangles), K (open magenta squares), p (red circles), and direct photon (open green crosses) v_2 as a function of p_T in (a) central 0–20% and (b) midcentral 20–40% Au+Au collisions at $\sqrt{s_{NN}} = 200$ GeV. Panels (c) and (d) show the v_2/n_q as functions of p_T/n_q for 0–20% and 20–40% respectively. Panels (e) and (f) show the v_2 scaled by the number of constituent quarks, n_q, as a function of KE_T/n_q, again for 0–20% and 20–40% centralities. For direct photons, $n_q = 2$ is assumed. In panels (a), (c), and (e), the 0–20% v_2 values are scaled by 1.6 for better comparison with the 20–40% results. Error bars and shaded boxes around points represent their statistical and systematic uncertainties, respectively [4,20].

and KE_T are also presented assuming that the n_q value for direct photons is 2. The agreement between the scaled direct photon v_2 and the pion, kaon, and proton data is impressive despite the large systematic error bars on the direct photon measurement. The scaled pions, kaons, protons, and photons agree at low KE_T/n_q in both centralities. At KE_T/n_q above 1.7 GeV, the direct photon's scaled v_2 drops below the pion values. This deviation can be understood as the result of the increased photon production by initial hard processes [4]. Of particular note is how the direct photon and proton v_2/n_q track together as they deviate from the pion values in the 20–40% centrality bin. This suggests a similar transition to the high-p_T hard scattering region for the scaled protons and photons. While the 0–20% proton v_2 does not extend high enough in KE_T/n_q, protons in the 0–20% centrality are also expected to break n_q-scaling at high KE_T/n_q and deviations are seen in the 10–20% bin [20].

A χ^2 analysis is undertaken to determine if $n_q = 2$ best produces the agreement between the direct photon and the n_q-scaled identified hadron v_2 data. This is done in two ways. In Sec. II A, the datasets are compared directly. In Sec. II B, the n_q-scaled identified hadron v_2 are fit and the direct photon v_2 are compared to that function.

A. χ^2 comparison between the direct photon and n_q-scaled hadron data

A χ^2 comparison is performed between the v_2 for direct photons to the n_q-scaled hadron data. The χ^2 comparison of the direct photon and identified hadron data is calculated according to

$$\chi^2 = \sum_{\text{Cent.}} \sum_{\pi,K,p} \sum_{KE_T/n_q} \frac{(v_{2\gamma}/n_{q\gamma} - v_{2h}/n_q)^2}{(\sigma_\gamma/n_{q\gamma})^2 + (\sigma_h/n_q)^2}, \qquad (1)$$

where $v_{2\gamma}$ is the direct photon v_2, v_{2h} is the identified hadron v_2 for each of the summed hadrons, π, K and p. The χ^2 is summed over the 0–20% and 20–40% centralities comparing the n_q-scaled pion, kaon and proton v_2/n_q values to the direct photon $v_2/n_{q\gamma}$ where $n_{q\gamma}$ is the only parameter. Determining the photon and hadron uncertainties, σ_γ and σ_h, is complicated because the published systematic errors for both the direct photons and identified hadrons combine both point-to-point and correlated systematic errors [4,20]. To address this the χ^2 analysis is performed in two ways. In one case, the quadrature sum of the statistical and systematic errors for direct photons and the identified hadron uncertainties is used, $\sigma = \sigma_{\text{stat}} \oplus \sigma_{\text{sys}}$. This assumes that the systematic errors are uncorrelated. Another χ^2 analysis assumes that the systematic errors are fully correlated and the photon and hadron uncertainties are limited to their statistical errors, $\sigma = \sigma_{\text{stat}}$. In both cases, the comparison of a given pair of direct photon and hadron data points are included in the χ^2 calculation only if the KE_T/n_q values are within 0.1 GeV/c of each other. An example of this data comparison over the full range in KE_T/n_q is shown in Fig. 4 where the photon-to-identified hadron data comparison plots with $n_{q\gamma} = 2$ are presented. A χ^2 of 16.28 is calculated using the quadrature sum of the statistical and systematic errors for the photon and hadron uncertainties with 35 degrees of freedom, NDF, and a reduced χ^2, χ^2/NDF, of 0.47 is found. As a result of requiring photon-hadron matching in KE_T/n_q, the number of degrees of freedom of the χ^2 calculation changes as $n_{q\gamma}$ varies. This leads to a discontinuous χ^2 distribution as a function of $n_{q\gamma}$, as seen in Fig. 5.

Figure 5(a) shows χ^2 versus $n_{q\gamma}$ when statistical and systematic errors are used to determine the χ^2 and Fig. 5(b)

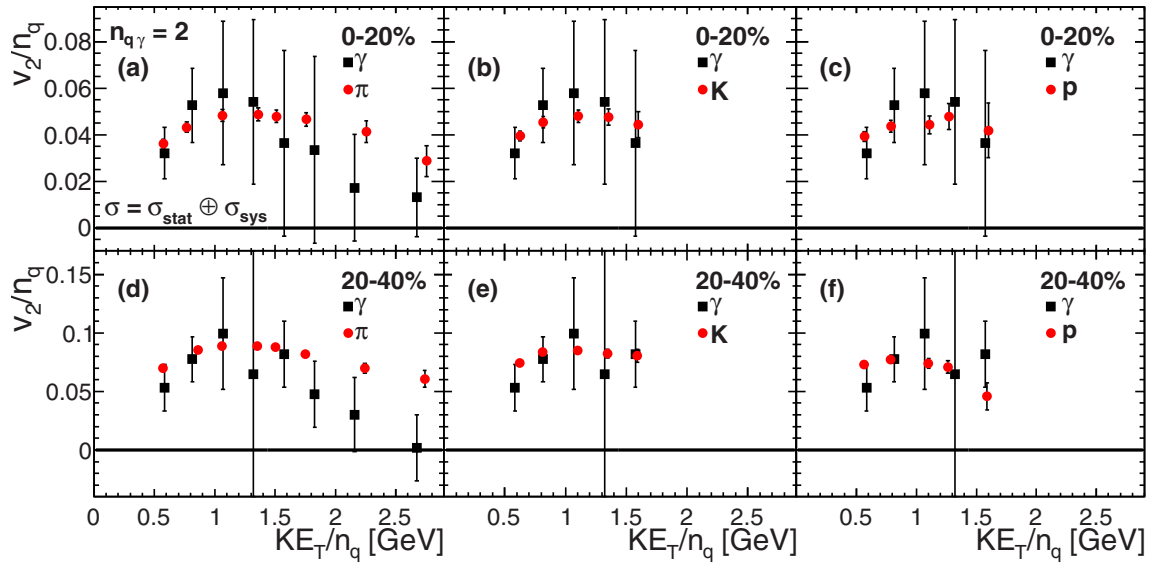

FIG. 4. (Color online) Example plots of the input data used for the calculation of χ^2 comparing the v_2/n_q vs KE_T/n_q for identified hadrons (red circles) [20] and direct photons (black squares) [4] using the quadratic sum of the statistical and systematic errors. Here, $n_{q\gamma} = 2$ is assumed for direct photons. The 0–20% (top row) and 20–40% (bottom row) $\sqrt{s_{NN}} = 200$ GeV Au+Au results are shown. Pions (left column), kaons (middle column), and protons (right column) are separately plotted with the direct photon data over the full KE_T/n_q range. The data are included in the χ^2 calculation only if the identified hadron and direct photon KE_T/n_q values are within 0.1 GeV/c. The χ^2 is calculated using the variation between direct photon and identified hadron v_2/n_q in all six plots. Error bars represent the statistical and systematic uncertainties summed in quadrature. A χ^2/NDF of 16.28/35 = 0.47 is found using the full KE_T/n_q range available in the data.

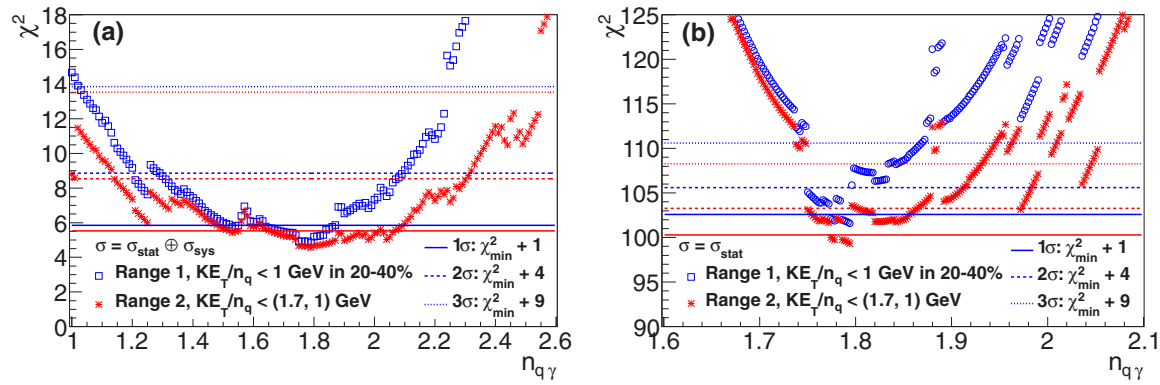

FIG. 5. (Color online) χ^2 distribution as a function of $n_{q\gamma}$ calculated using (a) the quadrature sum of the statistical and systematic errors for the hadron and photon uncertainties and (b) only the statistical errors. The χ^2 calculation with an upper limit of $KE_T/n_q < 1.0$ GeV in the 20–40% centrality bin is shown with blue open squares; this is range 1. The calculation with upper limits of 1.7 and 1.0 GeV in the 0–20% and 20–40% centrality bins, respectively, is shown with red $*$ marks; this is range 2. Horizontal lines are drawn at the location of the $\chi^2_{min} + 1$ (solid), $\chi^2_{min} + 4$ (dashed) and $\chi^2_{min} + 9$ (dotted) for each calculation.

shows χ^2 when only statistical errors are included. Open squares identify the χ^2 values when an upper limit of $KE_T/n_q < 1$ GeV is applied in the 20–40% centrality bin. This is range 1. It removes the region where the proton and pions deviate from n_q scaling [20]. Another χ^2 comparison, shown with $*$ marks and referred to as range 2, restricts the KE_T/n_q range in both centrality bins with upper limits of 1.7 and 1.0 GeV for the 0–20% and 20–40% centralities, respectively. This extends the KE_T/n_q cut to central collisions where n_q scaling is expected to remain broken [20]. When the KE_T/n_q range is restricted, the width of the χ^2 distribution increases reflecting the reduced resolving power of the χ^2 comparison when fewer data points are included.

The optimal $n_{q\gamma}$ values for n_q scaling are located at the χ^2 minima, a value of 1.79 for all four χ^2 data comparisons. The error on the $n_{q\gamma}$ parameter is related to the width of the χ^2 curve. It is determined from the range of $n_{q\gamma}$ values where χ^2 is below $\chi^2_{min} + 1$ for the 1σ limit, $\chi^2_{min} + 4$ for the 2σ limit, and $\chi^2_{min} + 9$ for the 3σ limit. Horizontal lines are drawn at the $\chi^2_{min} + n$ values in Fig. 5 with solid lines for the 1σ limits, dashed lines for the 2σ limits and dotted lines for the 3σ limits. When the systematic errors are assumed to be fully correlated, the $\sigma = \sigma_{stat}$ case, the n_q systematic error from the correlation must also be obtained. The systematic error on the $n_{q\gamma}$ in the $\sigma = \sigma_{stat}$ case is found by shifting all of the photon and identified hadron v_2 values to the extreme maximum or minimum values in their systematic error ranges, recalculating the χ^2 in the $n_{q\gamma}$ space, and determining the $n_{q\gamma}$ where χ^2 reaches a minimum value. The optimal $n_{q\gamma}$ values and errors from this comparison of data points are shown with their respective χ^2/NDF in Table II.

B. χ^2 analysis using fit to n_q-scaled hadron data

Here, a fit to the n_q-scaled identified hadron data is used to describe the universal scaling distribution. The 0–20% and 20–40% direct photon data are then compared to this function and fit using TMinuit to find the optimal $n_{q\gamma}$ by minimizing the χ^2,

$$\chi^2 = \sum_{\text{Cent.}} \sum_{KE_T/n_q} \frac{(v_{2\gamma}/n_{q\gamma} - v_{2\text{fit}})^2}{(\sigma_\gamma/n_q)^2}, \tag{2}$$

where $v_{2\gamma}$ is the direct photon v_2 and $v_{2\text{fit}}$ is the fit to the n_q-scaled identified hadron v_2. The χ^2 is summed over the 0–20% and 20–40% centralities comparing the $v_{2\text{fit}}$ to the direct photon $v_2/n_{q\gamma}$ where $n_{q\gamma}$ is the only parameter. Again, the χ^2 minimization is performed in two cases to address how the direct photon uncertainty σ_γ relates to the direct photon systematic errors. One case uses the quadrature sum of the statistical and systematic errors for direct photons, $\sigma = \sigma_{stat} \oplus \sigma_{sys}$. This assumes the systematic errors are uncorrelated. The second case assumes that the systematic errors are fully correlated and the photon uncertainties are limited to the statistical errors, $\sigma = \sigma_{stat}$.

To obtain $v_{2\text{fit}}$, the n_q-scaled identified hadron data are fit using a scaled probability density function of the Γ distribution,

$$G(x) = A \frac{[(x-\mu)/\beta]^{\gamma-1} e^{-1(x-\mu)/\beta}}{\beta\Gamma(\gamma)}, \tag{3}$$

where x is KE_T/n_q, γ is the shape parameter, μ is the location parameter, β is the scale parameter, A is an overall normalization scale. and $\Gamma(\gamma)$ is the gamma distribution $\Gamma(x) = \int_0^\infty t^{x-1} e^{-t} dt$. Figure 6 shows the fit results when the 0–20% and 20–40% Au+Au identified hadron v_2/n_q data are fit to Eq. (3). In the 20–40% centrality bin, high KE_T/n_q protons that deviate from the n_q-scaled pions are excluded from the fit and are not shown. Table I lists the parameters obtained from the fits for both centrality bins.

A TMinuit fit is used to determine the $n_{q\gamma}$ where the χ^2 from Eq. (2) reaches its minimum value. This fit is performed over two ranges. Range 1 removes the region where the proton breaks the n_q scaling [20] by applying an upper limit at $KE_T/n_q < 1$ GeV in the 20–40% centrality bin. Range 2 restricts the KE_T/n_q range in both centrality bins with upper limits of 1.7 and 1.0 GeV for the 0–20% and

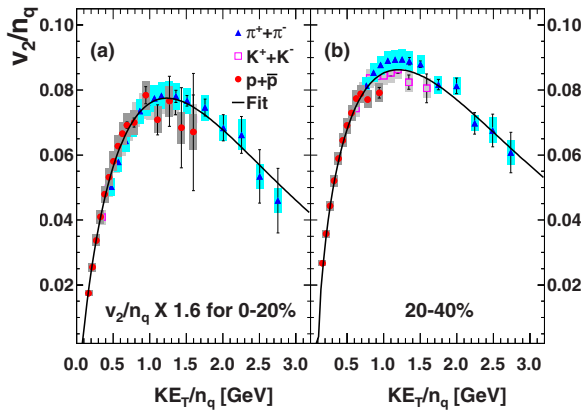

FIG. 6. (Color online) 0–20% and 20–40% Au+Au v_2/n_q vs KE_T/n_q for pions, kaons, and protons fit with a probability density distribution of a Γ function. High-p_T protons that deviate from n_q scaling in the 20–40% centrality bin are excluded from the fit and are not shown [20].

20–40% centralities, respectively. This removes the region in the 0–20% bin where n_q scaling is expected to be broken [20]. TMinuit finds the optimal $n_{q\gamma}$ value with statistical errors. When the direct photon systematic errors are assumed to be fully correlated, the $\sigma = \sigma_{\rm stat}$ case, the $n_{q\gamma}$ systematic errors from this correlation must also be determined. This is done by shifting the direct photon v_2 values to the extreme maximum and minimum of the systematic error range and refitting with TMinuit to find $n_{q\gamma}$ at the χ^2 minimum value. The resulting $n_{q\gamma}$ values and errors from the TMinuit fits are shown in Table II with their respective χ^2/NDF.

The low χ^2/NDF values under the $\sigma_\gamma = \sigma_{\rm stat} \oplus \sigma_{\rm sys}$ heading reflect the overestimation of the photon and hadron uncertainties when uncorrelated systematic errors are assumed. Under the $\sigma_\gamma = \sigma_{\rm stat}$ heading, when only the statistical errors are used in the χ^2 determination, the corresponding χ^2/NDF values are above unity, a consequence of the underestimation of the uncertainty when the systematic errors are assumed to be fully correlated. The separation of the systematic errors into errors that are point-to-point independent and those that are correlated is needed in order to fully interpret the χ^2/NDF values in these comparisons.

The hypothesized value of $n_{q\gamma} = 2$ is within the systematic uncertainty region when $n_{q\gamma}$ is determined from the data with $\sigma_\gamma = \sigma_{\rm stat}$ in both ranges 1 and 2. The $n_{q\gamma} = 2$ condition is inside of the 1σ limit for the $\sigma_\gamma = \sigma_{\rm stat} \oplus \sigma_{\rm sys}$, range 2 data comparison and within the 2σ limit for the $\sigma_\gamma = \sigma_{\rm stat} \oplus \sigma_{\rm sys}$, range 1 data comparison. The $n_{q\gamma}$ values from the comparison

TABLE I. Parameter values of a probability density distribution of a Γ function [see Eq. (3)] obtained from a fit to the Au+Au v_2/n_q vs KE_T/n_q data.

Parameters	0–20%	20–40%
γ	1.86	1.62
μ	0.08	0.11
β	1.34	1.76
A	0.166	0.34

to the fit of the n_q-scaled hadron data are very similar to the direct data comparison results. An $n_{q\gamma}$ value close to 1.8 is found over both ranges when $\sigma = \sigma_{\rm stat}$ is assumed and in range 2 when $\sigma = \sigma_{\rm stat} \oplus \sigma_{\rm sys}$ is assumed. Only the TMinuit fit over range 1 produces a $n_{q\gamma}$ value that differs from 1.8; however, it is within 2σ of the $n_{q\gamma} = 2$ hypothesis. Of the eight $n_{q\gamma}$ searches presented here, six are consistent with $n_{q\gamma} = 2$ within 1σ. The remaining two $n_{q\gamma}$ searches are consistent with the $n_{q\gamma} = 2$ hypothesis at the 2σ level. These two comparisons both use the larger KE_T/n_q region in the 0–20% centrality and $\sigma = \sigma_{\rm stat} \oplus \sigma_{\rm sys}$. These comparisons are affected by the difference between the pion v_2 and direct photon v_2 at $KE_T/n_q > 1.7$ GeV in the 0–20% centrality bin, seen in Fig. 3. This difference between the pion and direct photon v_2 at high KE_T/n_q may be the result of the increased direct photon contributions from hard scattering at high p_T, $p_T > 3.5$ GeV [4].

The large systematic errors in the direct photon data dominate the uncertainty in the $n_{q\gamma}$ determination. Reducing the systematic errors in the direct photon v_2 measurement and separating them into errors that are point-to-point independent and those that are correlated may reduce the uncertainty and improve the calculation of the χ^2 in these comparisons. Proton v_2 measurements that extend out to higher p_T in the 0–20% centrality bin, and direct photon v_2 measurements in additional centrality bins and collision systems would provide additional points for comparison, benefiting this analysis by reducing the width of the χ^2 distribution and improving the resolving power of the $n_{q\gamma}$ parameter. Furthermore, direct photon azimuthal anisotropy measurements at higher orders, v_n, will provide an additional test of this model. The model predicts that higher order direct photon v_n will follow the higher order modified n_q-scaling relation, with a universal curve in $v_n/n_q^{n/2}$ as a function of KE_T/n_q [19], with $n_{q\gamma} = 2$ for direct photons.

Seven out of the eight χ^2 comparisons shown here find an optimum $n_{q\gamma}$ value of approximately 1.8. In six cases, the $n_{q\gamma} = 2$ condition is within 1σ of the optimum value. In the remaining two cases, the $n_{q\gamma} = 2$ condition is within 2σ of the optimum value. It is believed that these two cases are biased by the hard scattering contributions at high p_T. These results, in conjunction with the similarity in the data seen in Fig. 3, indicate that the direct photon v_2 data are consistent with the hypothesis of $n_{q\gamma} = 2$ required by the q-$\bar{q}$ annihilation production mechanism.

III. SIMULATING THE DIRECT PHOTON v_2

To further develop the ansatz of photon production at confinement from coalescence-like quark–anti-quark annihilation, a data-driven Monte Carlo simulation is developed. The crux of the direct photon puzzle is to reconcile the p_T spectral shape with the large azimuthal anisotropy. In Sec. III A, the q-$\bar{q}$ photon p_T spectral shape and v_2 are simulated with a Monte Carlo simulation. Rather than calculating the yields, a fit to the measured p_T distribution is performed in Sec. III B to determine if the q-$\bar{q}$ photon p_T shape from the Monte Carlo is able to describe the large excess above the T_{AA}-scaled $p + p$ yield seen in the data. Then the direct photon v_2 is calculated by weighting the q-$\bar{q}$ photon v_2 by the relative contribution of the q-$\bar{q}$ photon component to the total direct photon yield; the T_{AA}-scaled $p + p$ contribution is assumed to be azimuthally isotropic.

TABLE II. Optimal $n_{q\gamma}$ values and errors with χ^2/NDF.

	$\sigma_\gamma = \sigma_{\rm stat} \oplus \sigma_{\rm sys}$		$\sigma_\gamma = \sigma_{\rm stat}$	
	$n_{q\gamma} \pm$ (stat)	χ^2/NDF	$n_{q\gamma} \pm$ (stat) $\pm$ (sys)	χ^2/NDF
Data, range 1	$1.79^{+0.08}_{-0.27}$	$4.85/20 = 0.24$	$1.79^{+0.002+0.67}_{-0.01-0.72}$	$101.6/20 = 5.1$
Data, range 2	1.79 ± 0.27	$4.53/17 = 0.27$	$1.79^{+0.002+1.09}_{-0.01-0.72}$	$99.5/17 = 5.9$
Fit, range 1	1.59 ± 0.22	$3.51/13 = 0.26$	$1.79 \pm 0.02^{+0.85}_{-0.68}$	$44.67/14 = 3.19$
Fit, range 2	1.83 ± 0.44	$1.55/5 = 0.31$	$1.88 \pm 0.07^{+1.18}_{-0.71}$	$34.14/6 = 5.68$

A. Monte Carlo of coalescence-like q-$\bar{q}$ photon v_2 production

The Monte Carlo consists of randomly sampling quark m_T values from a thermal blast-wave distribution. The quark flow is implemented by calculating the quark v_2 from a fit of the measured n_q-scaled identified hadron v_2 and then sampling the quark ϕ from the v_2-modulated ϕ distribution. This process is repeated for three quarks and then co-moving requirements are applied.

The quark m_T is randomly sampled from a thermal blast-wave distribution,

$$\frac{d^3N}{dm_T\,dy\,d\phi} \propto m_T^2 r \cosh(y) \times \exp\left(\frac{p_T \sinh(\rho)\cos(\phi) - m_T \cosh(\rho)\cosh(y)}{T}\right), \quad (4)$$

where T is the temperature, $m_T = \sqrt{p_T^2 + m_q^2}$ is the transverse mass, $\rho = \tanh^{-1}[\beta_S (r/R)^\alpha]$ is the boost angle, and ϕ is the azimuthal angle with respect to the reaction plane [23]. Further, β_S is the surface velocity, R is the maximum radius in the region, and m_q is the quark mass. A β_S value of 0.75 is assumed and is consistent with $\langle\beta\rangle = 0.5$ with α set to unity. A quark mass of 300 MeV, temperature of 106 MeV, and maximum radius of 8.5 fm are used. The parameters of the blast-wave distribution are taken from Refs. [24,25]. These blast-wave parameters characterize the m_T distribution of the late-stage medium and therefore identical parameters are used for the Au+Au 0–20% and 20–40% centrality bins. The r^2, y, and ϕ values that determine the blast-wave distribution are each chosen from flat distributions; r and y are the quark radius and rapidity, respectively. The quark y is chosen from ± 0.50, and a ± 0.35 rapidity cut is applied to the resulting photons. The random choice of ϕ ensures that each of the successive blast-wave distributions sample the full variation in azimuth.

Rather than using this ϕ for the quark ϕ, the thermal quark ϕ is chosen from a data-driven procedure to reduce the simulation's dependence on free parameters. This is done by using the m_T obtained from the blast wave to calculate the quark azimuthal anisotropy from a fit to the measured n_q-scaled v_2 of identified hadrons shown in Fig. 6. Once the quark v_2, v_{2q}, is calculated it is used to generate a $1 + 2v_{2q}\cos(2\phi)$ probability distribution to randomly select the quark ϕ. The v_{2q} is calculated using a fit to the measured n_q-scaled identified hadron v_2. A scaled probability density function of the Γ distribution, Eq. (3), is fit to the n_q-scaled identified hadron v_2 data as described in Sec. II B.

This method effectively averages the ϕ variation within the blast-wave distribution while still including radial boost effects. By choosing ϕ from the $1 + 2v_2\cos(2\phi)$ distribution, the measured identified hadron v_2/n_q is used to guide the modeled quark azimuthal anisotropy. This empirical approach to describe the quark azimuthal anisotropy keeps the number of free parameters in the model to a minimum. One downside of this approach is that the v_{2q} from the fit relies on the pion data at high KE_T/n_q which has increasing contributions from nonthermal quarks either from hard processes and fragmentation or from hard thermal coalescence [26]. This may underestimate the amount of quark flow at high KE_T/n_q.

The random determination of the quark m_T and ϕ is repeated for the second and third quarks within the Monte Carlo event. The same rapidity and radius is assumed for subsequent quarks, and therefore the same blast-wave distribution. However, a new m_T value is sampled, v_{2q} is calculated, and ϕ is sampled using the $1 + 2v_{2q}\cos(2\phi)$ distribution. The following co-moving requirements, motivated by [18], are applied to all three quarks to produce a baryon and to the first and second quarks to produce a meson:

$$\begin{aligned} \textbf{Mesons}: &|p_1 - p_2| < 2\Delta p, \quad |x_1 - x_2| < \Delta x \\ \textbf{Baryons}: &|p_1 - p_2| < \sqrt{2}\Delta p, \quad |x_1 - x_2| < \sqrt{2}\Delta x \\ &|p_1 + p_2 - 2p_3| < \sqrt{6}\Delta p, \\ &|x_1 + x_2 - 2x_3| < \sqrt{6}\Delta x \end{aligned}$$

where p_i and x_i are the three-dimensional momentum and position vectors of the various quarks, and Δp and Δx are 0.2 GeV/c and 0.85 fm, respectively [18]. Quarks and anti-quarks that annihilate to produce photons must satisfy the same co-moving requirements as mesons. The four-momenta of quark pairs and triplets that satisfy the co-moving requirements are summed to create pions, photons, and protons, respectively. The hadrons and photons are brought on mass shell while maintaining kinetic energy conservation. Figure 7 shows the amount of energy taken up by the gluon to bring the photon on mass shell as a function of the direct photon's KE_T for the 0–20% (a) and 20–40% (b) simulations. The z axis is the number of counts and is shown with a logarithmic color scale. The gluon's energy contribution, $E_{\rm Gluon}$, is defined as $E_\gamma - E_{q1} - E_{q2}$ and has a value of approximately -600 MeV. At photon $KE_T < 2$ GeV, $E_{\rm gluon}$ extends to lower energies of -770 MeV; however, the majority of the contribution is located at -600 MeV for all photon KE_T values. This negative value means that the gluon removes some of the energy from the quarks and passes it to the medium when the photon is

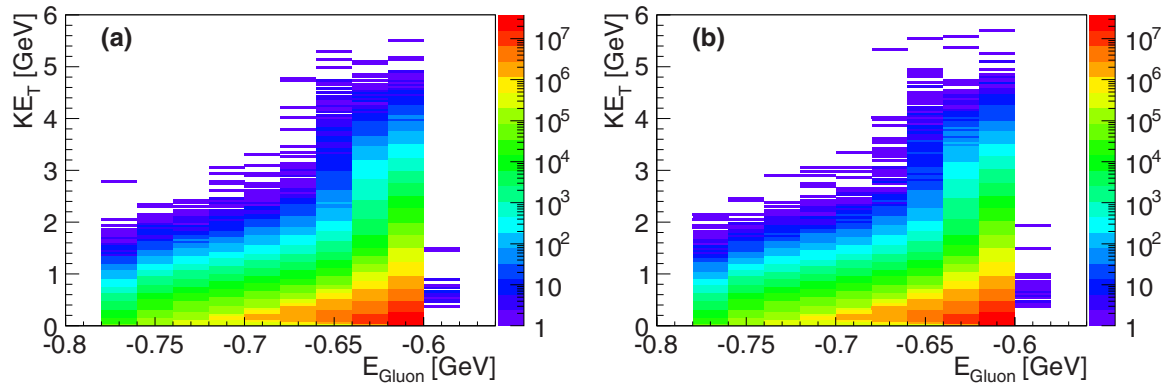

FIG. 7. (Color online) Energy taken by the gluon as a function of the direct photon's KE_T for the (a) 0–20% and (b) 20–40% simulations. The z axis is the number of counts and is shown with a logarithmic color scale.

produced. Additional simulations maintaining momentum conservation and energy conservation are also performed; however, kinetic energy conservation best reproduces the n_q scaling seen in the pion and proton v_2 data. Figure 8 shows the v_2 for the thrown quarks and simulated pions, protons, and photons in (a) 0–20% and (b) 20–40% centrality bins. The v_2/n_q vs KE_T/n_q, Figs. 8(c) and 8(d), show that n_q scaling is well reproduced in the simulation. Table III displays the inverse slopes of the Monte Carlo p_T spectral shape when fit to an exponential in different p_T ranges. These are consistent with the inverse slopes obtained from fits to the Au+Au data over similar p_T ranges [2,3].

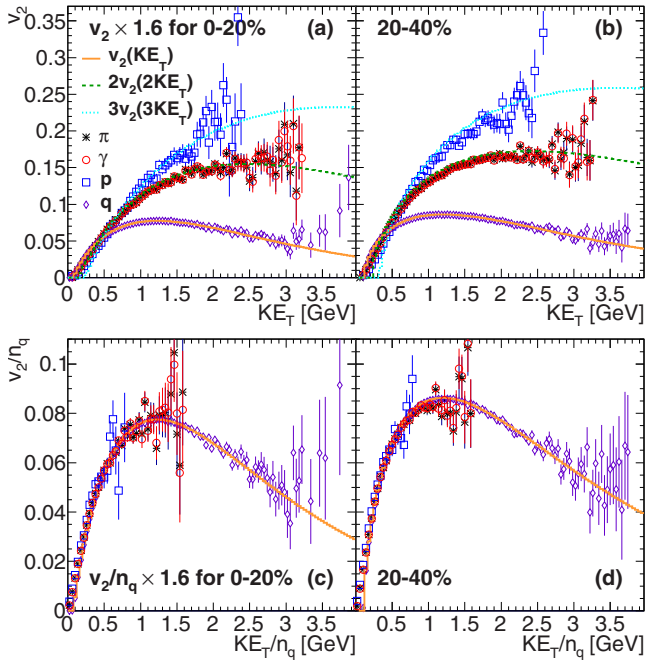

FIG. 8. (Color online) The v_2 for pions, photons, protons, and thrown quarks simulated using the fast Monte Carlo method. Plots (a) and (b) are the v_2 vs KE_T for the 0–20% and 20–40% respectively. Plots (c) and (d) are the n_q-scaled results for 0–20% and 20–40%. The 0–20% v_2 values are scaled by 1.6 to make the y-axis scales consistent.

B. Determining the yield of the q-$\bar{q}$ photon component

To find the total direct photon production, a two-component model consisting of the q-$\bar{q}$ photon contribution and the T_{AA}-scaled $p+p$ contribution is used. While additional photon sources are expected, these are assumed to be negligible compared to the q-$\bar{q}$ and T_{AA}-scaled $p+p$ components. The simulated q-$\bar{q}$ photon contributions are normalized to the measured direct photon yields. The normalization constant of the q-$\bar{q}$ photon component is determined from a fit to the measured Au+Au [2,3,27] and T_{AA}-scaled $p+p$ data [2,28,29] using TMinuit. The normalization constant is the only parameter of the fit. The χ^2 is calculated using the statistical errors from the Monte Carlo simulation and the statistical and systematic errors from the data summed in quadrature. At low p_T where $p+p$ reference data are scarce, the $p+p$ yield is extrapolated from the power law fit obtained from [3]. The normalization error on the q-$\bar{q}$ photon component and the systematic error of the T_{AA}-scaled $p+p$ fit result in a systematic error band on the simulation.

Figure 9 shows the resulting p_T distributions for 0–20% and 20–40% Au+Au collisions. The various Au+Au measurements are shown in red circular symbols and the T_{AA}-scaled $p+p$ measurements are shown in blue square and cross symbols. The $p+p$ fit is shown with a black hatched band, the normalized q-$\bar{q}$ photon contribution is shown with a cyan band, and the total simulated yield is shown with a purple band. The error on the yield determination results in a systematic band on the q-$\bar{q}$ photon contribution which is propagated to the total simulated yield. Below the main figures the ratio of the Au+Au data to the simulation result is shown. This ratio is fit to a flat line and found to be consistent with one for both centralities, a value of 0.951 ± 0.051 for 0–20% and 1.038 ± 0.065 for 20–40%. The χ^2/NDF values for these

TABLE III. Inverse slope of the direct photon p_T spectral shape in different centralities and p_T ranges (in GeV/c).

Centrality	p_T range	Monte Carlo	Au+Au data [2,3]
0–20%	0.6–2.0	233 ± 6	$239 \pm 29 \pm 7$
0–20%	1.0–2.2	251 ± 8	$221 \pm 19 \pm 19$
20–40%	0.6–2.0	233 ± 8	$260 \pm 33 \pm 8$
20–40%	1.0–2.2	251 ± 10	$217 \pm 18 \pm 16$

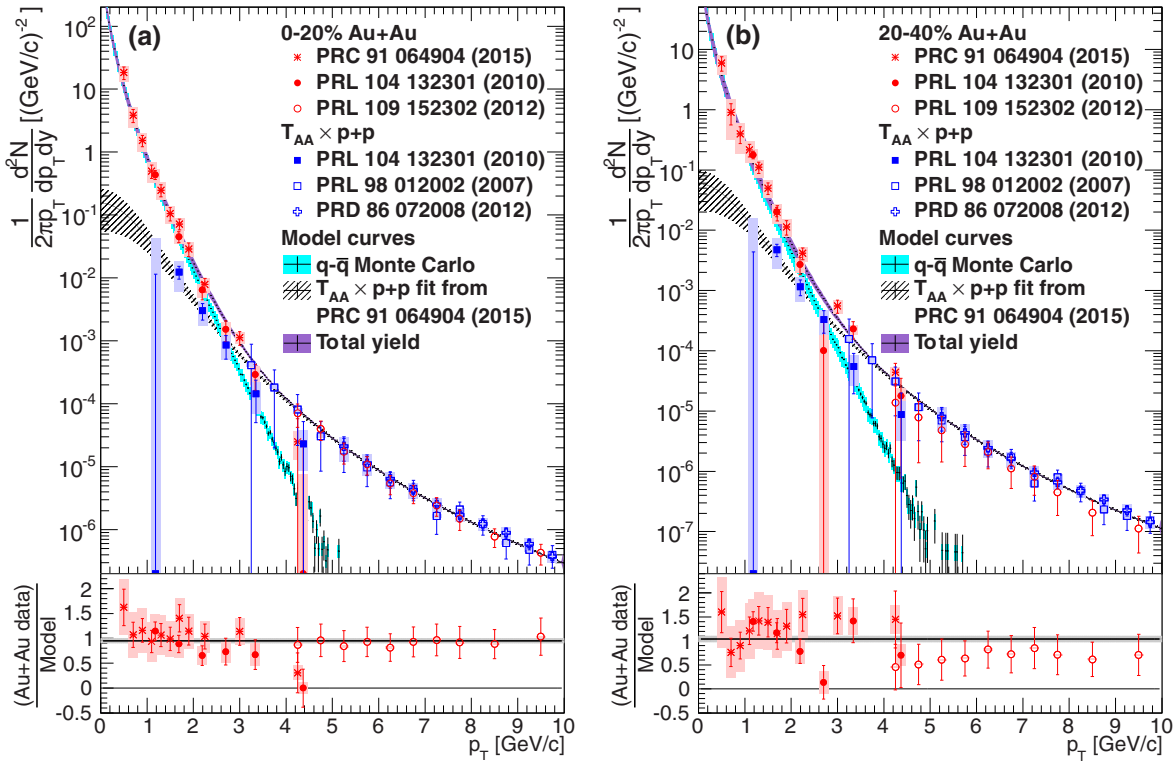

FIG. 9. (Color online) Direct photon yield versus p_T for the (a) 0–20% and (b) 20–40% Au+Au data (red circles and asterisks) [2,3,27] on a $\log_{10}$ scale. The T_{AA}-scaled $p+p$ yields (blue squares and crosses) [2,28,29] are also shown including a power law fit to the $p+p$ data (black diagonal hatched band) [3]. The Monte Carlo yield from quark-anti-quark annihilation (cyan band) are fit to the data and are shown with the total fit yield (purple band) found by summing the Monte Carlo yield and the T_{AA}-scaled $p+p$ fit. The ratio of the Au+Au data over the total fit yield is shown in the lower plots. The thick black line is a flat line fit to this ratio with a value of 0.951 ± 0.051 and 1.038 ± 0.065 for the 0–20% and 20–40% ratios, respectively.

flat line fits are $22.8/26 = 0.877$ and $32.5/26 = 1.25$ for the 0–20% and 20–40% ratios, respectively. This confirms that the photons generated by the gluon-mediated annihilation of radially boosted quarks are able to describe the shape of the direct photon p_T spectra for both the 0–20% and 20–40% centrality bins.

The total direct photon v_2 is the weighted average of each component's v_2. The T_{AA}-scaled $p+p$ contribution is

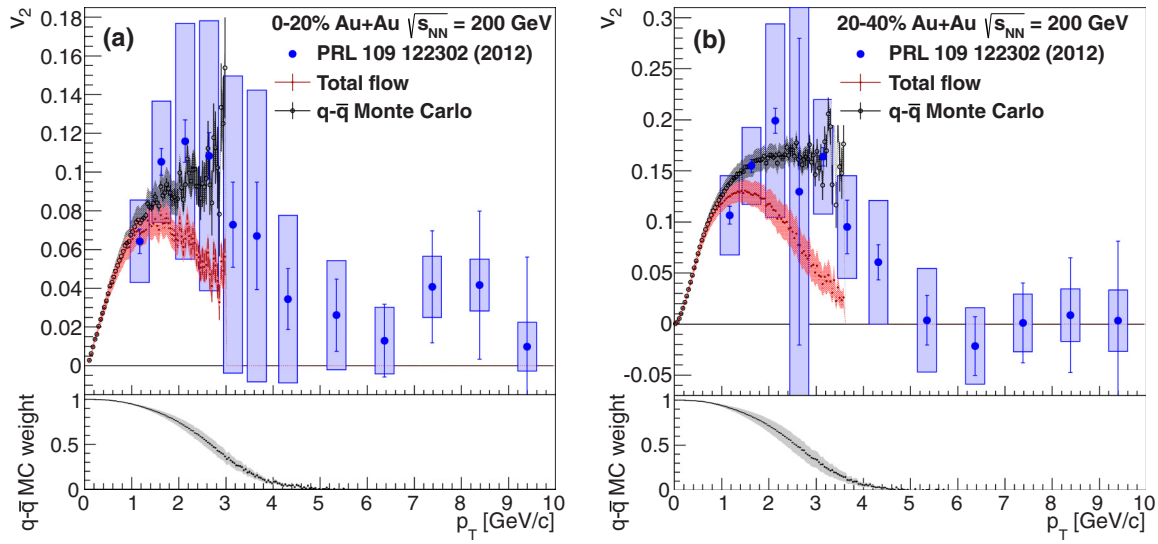

FIG. 10. (Color online) Direct photon v_2 versus p_T for the (a) 0–20% and (b) 20–40% Au+Au data (blue circles) [4]. The Monte Carlo v_2 from quark–anti-quark annihilation (black open circles) and the total v_2 (small red closed circles) are also shown. The relative contribution of the quark–anti-quark annihilation component is shown in the lower plot of each figure.

assumed to have no reaction plane dependence and, therefore, a v_2 of zero. By weighting the simulated q-$\bar{q}$ photon v_2 by the relative contributions of the q-$\bar{q}$ photon yield to the total simulated yield, the total low-p_T photon v_2 for each centrality can be calculated. Figure 10 compares the simulated direct photon v_2 to the measured Au+Au v_2 (solid blue circles) [4]. The open black circles are the unweighted q-$\bar{q}$ photon v_2 generated in the Monte Carlo. The small red closed circles are the total direct photon v_2 assuming uniform azimuthal production from the T_{AA}-scaled $p+p$ source. The relative contribution of the q-$\bar{q}$ photon component to the yield is shown below the v_2 plots; this is the weight used to calculated the total simulated v_2. The error in the q-$\bar{q}$ yield normalization led to the systematic error in this q-$\bar{q}$ Monte Carlo weight. The systematic error in the modeled v_2 is calculated from the quadrature sum of this normalization error and the systematic error on the fit to the n_q-scaled v_2 of identified hadrons, with relative error values of 10% and 7% in 0–20% and 20–40%, respectively. The model simulation of the total direct photon v_2 extends out to a p_t of 3.2 GeV/c in 0–20% and 3.6 GeV/c in 20–40%, above which the simulation lacks sufficient statistics. For the 0–20% centrality the total direct photon v_2 agrees with the measured results within error bars. However, above a p_T of 1.4 GeV/c, the simulated v_2 is systematically at the bottom of the error range. In the 20–40% centrality comparison, the total simulated v_2 agrees with the measured results for p_T less than 3 GeV/c; above 3 GeV/c it underestimates the measured v_2. In both centralities, the simulated direct photon v_2 agrees with the measured v_2 within errors.

IV. CONCLUSIONS

Photon production from gluon-mediated q-$\bar{q}$ annihilation as the system becomes color neutral is proposed as a large additional source of direct photons. This would require direct photons follow n_q scaling with an $n_{q\gamma} = 2$. The large direct photon flow measured in Au+Au collisions at RHIC is consistent with n_q scaling when $n_{q\gamma} = 2$. Furthermore, in the 20–40% comparison where the high-p_T proton v_2/n_q is seen to split from the n_q-scaled pion result, the direct photon v_2/n_q follows the same trend as the proton. This suggests that direct photons and protons may experience similar transitions from the recombination-dominated intermediate p_T to the higher p_T region dominated by hard processes. χ^2 comparisons of the direct photon and identified hadron v_2 in KE_T/n_q regions where n_q scaling is seen in identified hadron data, find that the direct photon v_2 optimally agrees with the uniform n_q-scaled curve when $n_{q\gamma}$ is near a value of 1.8. Six out of eight of χ^2 comparisons are consistent with $n_{q\gamma} = 2$, the remaining two comparisons are consistent at the 2σ level. The two remaining comparisons include the 0–20% high KE_T/n_q region where deviations from n_q scaling are expected. The χ^2 comparisons would benefit from reduced systematic errors on the direct photon v_2 measurement and the separation of the systematic errors into uncorrelated and correlated errors. Direct photon and identified hadron v_2 measurements in additional centralities, $\sqrt{s_{NN}}$, and collisions systems as well as proton v_2 measurements that extend out to higher p_T would provide further points of comparison and thus improve this analysis.

A Monte Carlo simulation generates the q-$\bar{q}$ annihilation photon component p_T shape and ϕ modulation assuming a coalescence-like framework with quarks that follow a blast-wave m_T distribution and a data-driven v_2 parametrization. The Monte Carlo is able to reproduce the n_q scaling of pions and protons and determine the q-$\bar{q}$ photon v_2 and the shape of its p_T distribution. The resulting q-$\bar{q}$ photon p_T shape with the T_{AA}-scaled $p+p$ photon yield is able to describe the large direct photon excess seen in 0–20% and 20–40% Au+Au collisions. The simulated direct photon v_2 is consistent with the measured v_2 in the 0–20% centrality bin but systematically low. In the 20–40% comparison the simulated direct photon v_2 is able to reproduce the measured direct photon v_2 at p_T less than 3 GeV/c but underestimates the v_2 at higher p_T as the T_{AA}-scaled $p+p$ contribution becomes significant. The addition of thermal hard quark pairs would likely contribute to additional yield and flow for p_T values above 3 GeV/c [26]. Future work would benefit from a more robust hydrodynamic calculation of the flowing quarks near the phase transition with yield estimates. This is particularly important because the determination of the quark v_2 from the n_q-scaled identified hadron v_2 is expected to falter at high p_T as nonthermal production mechanisms such as thermal hard coalescence and fragmentation from hard interactions contribute to the pion yield.

This paper has focused on the published $\sqrt{s_{NN}} = 200$ GeV Au+Au 0–20% and 20–40% direct photon p_T and v_2 distributions. Future work to simulate the q-$\bar{q}$ photon contributions in more peripheral collisions is promising. Additionally, the higher orders of the direct photon flow present a new quantity to distinguish between the different photon processes. Given the soft-gluon-mediated q-$\bar{q}$ annihilation production mechanism ansatz, the v_n for direct photons is expected to be similar to the pion v_n at p_T less than 3 GeV/c for higher orders of n. This model predicts that higher order v_n n_q-scaling laws seen with identified hadrons [19] will remain valid for the direct photon v_n where the $n_{q\gamma} = 2$.

ACKNOWLEDGMENTS

The author thanks John Lajoie and Paul Stankus for many valuable conversations. Additional discussions with W. A. Zajc, Peter Steinberg, Anne Sickles, Rich Petti, Volker Koch, and Che-Ming Ko are also recognized as are the organizers and attendees at the 2013 ECT* workshop on Electromagnetic Probes of Strongly Interacting Matter: Status and Future of Low-Mass Lepton-Pair Spectroscopy. This research was supported by US Department of Energy Grants No. DE-FG02-86ER40281 and No. DE-FG02-92ER40692.

[1] C. Klein-Boesing, Ph.D. thesis, University of Muenster, 2005.
[2] A. Adare *et al.*, Phys. Rev. Lett. **104**, 132301 (2010).
[3] A. Adare *et al.*, Phys. Rev. C **91**, 064904 (2015).
[4] A. Adare *et al.*, Phys. Rev. Lett. **109**, 122302 (2012).
[5] M. Wilde (for the ALICE Collaboration), Nucl. Phys. A **904**, 573c (2013).

[6] D. Lohner (for the ALICE Collaboration), J. Phys. Conf. **446**, 012028 (2013).
[7] R. Chatterjee, E. S. Frodermann, U. Heinz, and D. K. Srivastava, Phys. Rev. Lett. **96**, 202302 (2006).
[8] R. Chatterjee and D. K. Srivastava, Phys. Rev. C **79**, 021901 (2009).
[9] F.-M. Liu, T. Hirano, K. Werner, and Y. Zhu, Phys. Rev. C **80**, 034905 (2009).
[10] F.-M. Liu and S.-X. Liu, Phys. Rev. C **89**, 034906 (2014).
[11] B. Müller, S.-Y. Wu, and D.-L. Yang, Phys. Rev. D **89**, 026013 (2014).
[12] K. Tuchin, Phys. Rev. C **87**, 024912 (2013).
[13] M. Chiu, T. K. Hemmick, V. Khachatryan, A. Leonidov, J. Liao, and L. McLerran, Nucl. Phys. A **900**, 16 (2013).
[14] H. van Hees, C. Gale, and R. Rapp, Phys. Rev. C **84**, 054906 (2011).
[15] O. Linnyk, W. Cassing, and E. L. Bratkovskaya, Phys. Rev. C **89**, 034908 (2014).
[16] S. S. Adler *et al.*, Phys. Rev. Lett. **91**, 182301 (2003).
[17] D. Molnar and S. A. Voloshin, Phys. Rev. Lett. **91**, 092301 (2003).
[18] V. Greco, C. M. Ko, and P. Levai, Phys. Rev. C **68**, 034904 (2003).
[19] A. Adare *et al.*, arXiv:1412.1038.
[20] A. Adare *et al.*, Phys. Rev. C **85**, 064914 (2012).
[21] A. Adare *et al.*, Phys. Rev. Lett. **98**, 162301 (2007).
[22] A. Adare *et al.*, arXiv:1412.1043.
[23] E. Schnedermann, J. Sollfrank, and U. Heinz, Phys. Rev. C **48**, 2462 (1993).
[24] Z. Tang, Y. Xu, L. Ruan, G. van Buren, F. Wang, and Z. Xu, Phys. Rev. C **79**, 051901(R) (2009).
[25] F. Retiere and M. A. Lisa, Phys. Rev. C **70**, 044907 (2004).
[26] R. C. Hwa and C. B. Yang, Phys. Rev. C **70**, 024905 (2004).
[27] S. Afanasiev *et al.*, Phys. Rev. Lett. **109**, 152302 (2012).
[28] A. Adare *et al.*, Phys. Rev. D **86**, 072008 (2012).
[29] S. S. Adler *et al.*, Phys. Rev. Lett. **98**, 012002 (2007).